DOI: https://doi.org/10.24425/amm.2024.149796

LONG ZHANG[1*], LIANG LIU[1], FEIHONG LIU[1], JIAN SUN[2*], DONGSHENG WANG[2]

EFFECT OF POST-HEAT TREATMENT ON THE MECHANICAL PROPERTIES AND CORROSION BEHAVIOR OF DUPLEX STAINLESS STEEL FABRICATED BY WIRE ARC ADDITIVE MANUFACTURING

In this study, the effect of heat treatment on the microstructure and mechanical properties of 2209 duplex stainless steel fabricated by wire arc additive was analyzed. It was found that solution treatment at 1100°C for 2 hours and tempering at 300°C for 2 hours can effectively improve the grain inhomogeneity of 2209 duplex stainless steel, eliminate γ_2 and harmful brittle phases, and take into account the mechanical properties and corrosion resistance. Compared with the original deposition state, the hardness and yield strength increased by 10% and 31.8% to 245.6 HV and 499.7 MPa, which meet the requirements of engineering propellers. Electron back-scattered diffraction studies showed that the grains became refined and austenite maintained <101>//Z orientation after solution heat treatment. Many small-angle grain boundaries were present in both the original sample and the solid solution, but further tempering transformed the small-angle grain boundaries into large-angle grain boundaries.

Keywords: arc additive manufacturing; 2209 duplex stainless steel; heat treatment; microstructure properties

1. Introduction

Duplex stainless steel (DSS) is a stainless steel with two phases austenite (γ) and ferrite (α), which has excellent mechanical properties and corrosion resistance compared to other stainless steels and therefore has a wide range of applications in petroleum and marine propulsion [1,2]. However, conventional DSS production requires a high-cost fabrication process for very complex shapes. Wire Arc additive manufacturing (WAAM), due to its efficient productivity and low cost, has attracted the attention of researchers [3-5].

WAAM is an additive manufacturing technique based on multilayer metal deposition, by which metal wires are processed and shaped by an electric arc heat source, resulting in higher material utilization than conventional manufacturing. Therefore, the WAAM process is preferred for manufacturing large and medium-sized complex geometry parts. At the same time, it has a higher deposition rate and is more cost-effective than powder-based additive manufacturing techniques [6]. However, high deposition rates also lead to the production of parts with defects such as cracks and shrinkage; because arc additive manufacturing is performed by layer-by-layer stacking, there are imbalances in the heating and cooling processes of each layer, which can lead to residual stresses and harmful equivalent defects within the material, and the presence of these defects can lead to lower mechanical properties of WAAM products than forged products [7]. Posch et al. [8] produced an impeller blade from ER2209 DSS using Cold Metal Transition Wire Arc Additive Manufacturing (CMT-WAAM). They found that the main problem in the DSS WAAM process was the presence of deleterious phases such as Cr2N, σ and χ phases, which made the tensile properties of the DSS produced by WAAM poor. Wu et al. [9] pointed out that the solidification mode of commonly used DSS (including 2205, 2209, and 2507) is $L \rightarrow \delta \rightarrow \delta + \gamma$. Therefore, the arc heat input must be controlled in the WAAM process to reduce the austenite ratio and balance the ferrite/austenite ratio. In response to the above problems, the scientists and technicians have mainly solved them by changing the process, developing new wires, and post-heat treatment. Zhang et al. [10] designs a new type of flux-cored wire for WAMM of DSS, and this wire arc additive duplex stainless steel (FCWA-AM DSS) produced by this flux-cored wire has significantly improved yield strength and ultimate tensile strength compared with WAAM DSS using ordinary wire. Moreover far beyond the rolling and casting DSS strength requirements. Wu et al. [9] found that variable polarity cold metal transfer (VP-CMT) could better control the

[1] ANHUI UNIVERSITY OF TECHNOLOGY, SCHOOL OF METALLURGICAL ENGINEERING, MA'ANSHAN 243002, CHINA
[2] TONGLING UNIVERSITY, KEY LABORATORY OF CONSTRUCTION HYDRAULIC ROBOTS OF ANHUI HIGHER EDUCATION INSTITUTES, TONGLING 244061, CHINA
* Corresponding authors: longzhang@ahut.edu.cn, sjxa0913@163.com

ferrite/austenite ratio of 2209 DSS. Nikam et al. [11] developed ER2594 super duplex stainless steel using CMT-WAAM, and the tensile properties in different directions (including horizontal, 45°, and vertical) with tensile properties superior to those of 6A SDSS in the cast state of ASTM A890 standard.

At present, studies on the mechanical properties of duplex stainless steels fabricated by the arc addition method mainly focus on the effects of different processes on the material tissue properties. In contrast, relatively few studies have been conducted on improving the mechanical properties of WAAM DSS by heat treatment. In addition, previous studies on heat treatment of DSS were mainly aimed at increasing the austenite content [12,13] or removing unfavorable secondary phases such as Cr2N and σ-phase [14]. The traditional approach to improve the mechanical properties of duplex stainless steels tends to solid solution treatment, which re-dissolves the precipitated phases into the matrix. The solid solution temperature during solid solution treatment not only changes the ratio of ferrite to austenite in duplex stainless steel but also leads to changes in the grain size of duplex stainless steel at different solid solution temperatures, and such tissue changes can have a significant impact on the mechanical properties of duplex stainless steel. Generally, the proportion of single phase in duplex stainless steel should not be less than 30%, and the corresponding solid solution temperature should be between 1100°C and 1300°C. Zhang et al. [15] performed a heat treatment of WAAM 2209 DSS. The results showed that the pitting properties of 2209 DSS were significantly improved by heat treatment of the solution at 1300°C for 1 h, followed by water quenching. Meanwhile, the crystal structure and microstructure indicated that the heat treatment at 1300°C could balance the ratio of the two phases and improve the mechanical properties of 2209 DSS. Therefore, an attempt is made in this study to improve the mechanical properties of WAAM DSS using heat treatment. The yield strength and tensile strength of WAAM 2209 duplex stainless steel were improved by using a new heat treatment (solution plus tempering), so that the yield strength of the heat-treated duplex stainless steel is ≥450 MPa and the tensile strength is ≥620 MPa, and at the same time there is better corrosion resistance, which meets the requirements of the application of a kind of engineering propeller material.

2. Experimental

As shown in Fig. 1(a, b), the material used for the experiments was 2209 DSS (Chemical composition of commercial raw wires: Ni 9, Si 0.8, Mn 0.9, Mo 3.2, Cr 22.7, C 0.03, N 0.13, Fe-bal wt-%) produced by arc additive manufacturing, and it can be seen that the samples have a good deposition effect. The intermediate zone – XOY surface was selected as the object of study. The effects on the structure and mechanical properties of 2209 DSS were investigated by different heat treatment processes, selecting the solid solution and low-temperature tempering temperature that do not change the austenite/ferrite ratio. The solid solution temperature used in the experiments was 1100°C, held for 1 h to ensure the removal of residual stresses, followed by water cooling. In contrast, the solid solution + tempering was 1100°C held in solid solution for 1 h, and then tempered at 300°C for 2 h.

In order to analyze the effect of heat treatment on the three sets of specimens, the middle region was selected for the study, and the sampling locations are shown in Fig. 1(c). Region "1" is the tensile specimen region, and the tensile specimen size is shown in Fig. 1(d), and region "2" is the other experimental characterization region. Small specimens with dimensions of

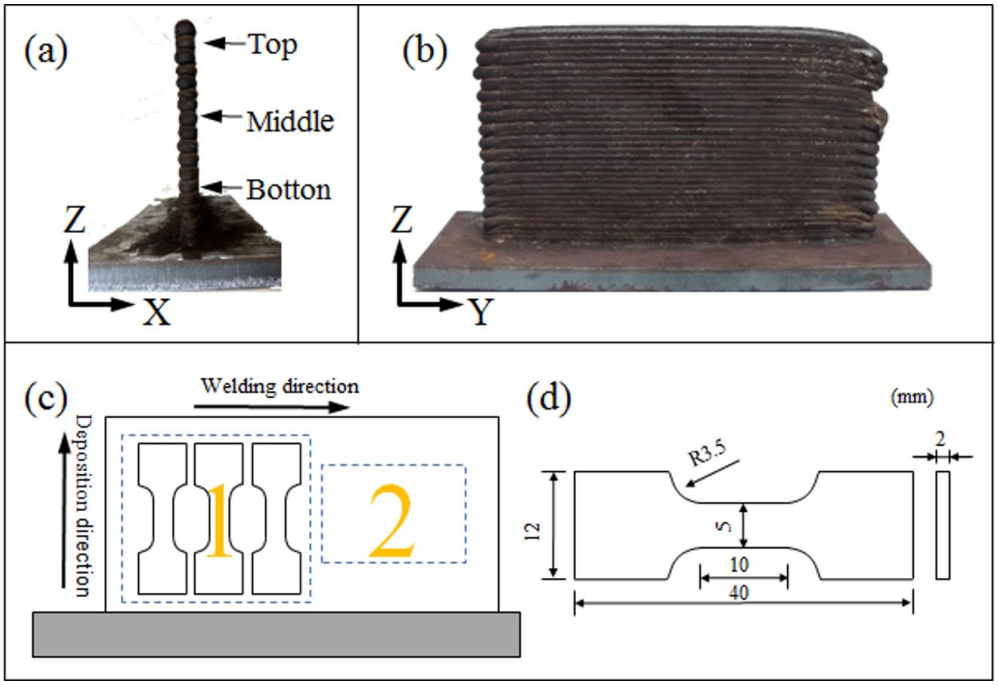

Fig. 1. (a, b) Photographs of the 2209 DSS thin-walled assembly made by WAAM in different orientations; (c) schematic diagram of a thin-wall component and the sample location; (d) tensile sample dimensions

10 mm × 10 mm × 7 mm were cut from three sets of specimens using a DK7735 EDM wire cutter. The samples were ground and polished, etched using ferric chloride hydrochloride solution (5 g FeCl3 + 50 ml HCl + 50 ml H2O), and observed metallographically using an OLYMPUS BX51 optical microscope (OA). The electron back-scattered diffraction (EBSD) experiment first electrolyzed the polished sample in a 10% room temperature oxalic acid electrolyte at 15 V for 50 s. After the surface was bright and free of scratches, it was observed with a SIGMA 500 scanning electron microscope, measuring an area of 500 μm × 500 μm in steps of 1.5 μm, and the experimental data were processed with channel5. The electrochemical experiments were performed on a CHI-760E constant potential meter with a test solution of 3.5 wt% NaCl at 25°C and a 10 mV/min scan rate. A saturated calomel electrode (SCE) was used as a reference electrode, a platinum sheet was used as an auxiliary electrode, and the specimen was used as a working electrode. The hardness of the specimens was measured using an HV-1000 microhardness tester with a load of 200 g and a duration of 15 s. According to GB/T228.1-2010 Standard for Tensile Testing of Metallic Materials, the tensile tests were performed on a WNW-30G testing machine at a constant tensile speed of 1 mm/min at room temperature, and then the fracture morphology of the samples was observed using a JSM-6490LV SEM scanning electron microscope. Three specimens measuring 10 mm × 10 mm × 0.3 mm were cut from different samples, mechanically thinned to 50 μm, and then thinned to 10 μm using a Gatan 695 precision ion polish in system. The bright-field was observed using an FEI Talos F200S G2 transmission electron microscopy (TEM).

3. Results

3.1. Microstructural characterization

Fig. 2 shows the microstructure of WAAM 2209 DSS under different heat treatments, indicating that austenite is distributed on the ferrite matrix. 2209 DSS generally has four different forms of austenite, grain boundary austenite (GBA) located at the ferrite grain boundaries, Weiss austenite (WA) extending towards the inner ferrite grain boundaries, intragranular austenite (IGA) with inhomogeneous nucleation inside the ferrite grain boundaries, and secondary austenite (γ_2). GBA, WA and IGA are also known as primary austenite [16]. As shown in Fig. 2, in the deposited state, the size grains of austenite are inhomogeneous, and the WA and IGA grains are large, which is detrimental to the performance. Also present is γ_2, formed during the heat input of subsequent layers in arc additive manufacturing. Although its grain size is much smaller than that of the native austenite, γ_2 is often accompanied by the generation of deleterious phases, such as the σ phase [17]. After the solid solution and tempering heat treatments, the organization becomes homogeneous and the deleterious phases at the austenite grain boundaries are significantly reduced. According to the phase diagram [15], it was found that at the temperature chosen for a solid solution, the ferrite matrix still belongs to the supersaturated state, austenite still by the increasing trend, γ_2 merged with other austenite grows, or grows by itself, there is much tiny intragranular austenite.

The inverse pole figure of the Z-direction (IPF-Z) of the sample austenite is shown in Fig. 3. In the samples with deposited

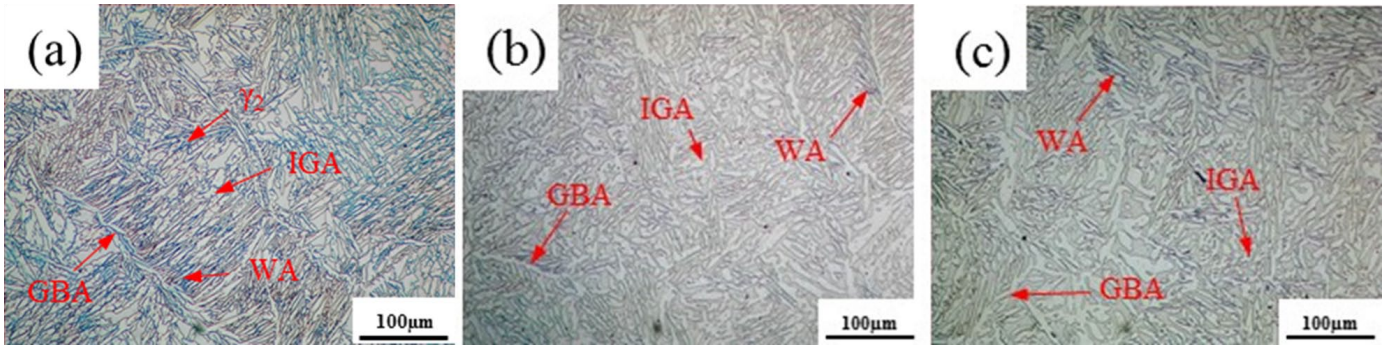

Fig. 2. Microstructure of the (a) as-deposited, (b) solid solution, (c) solid solution + tempering

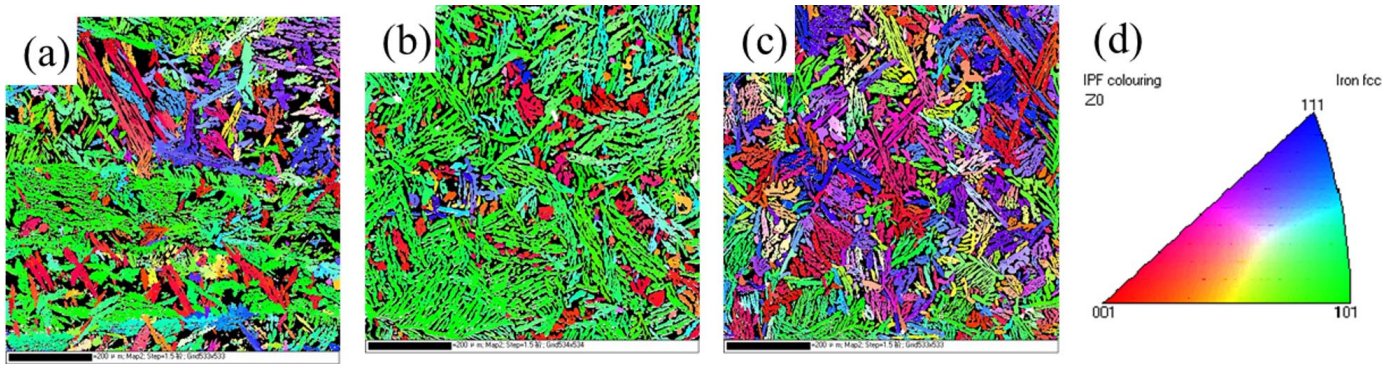

Fig. 3. IPF-Z of (a) as-deposited, (b) solid solution, (c) solid solution + tempering

and solid solution EBSD, most of the austenite is green, indicating that it has <101> // Z texture. However, there is no obvious crystal orientation for the tempered samples.

The grain boundary characteristic diagram of the sample is shown in Fig. 4. The grain boundaries can be divided into low-angle grain boundaries (LAGBs) and high-angle grain boundaries (HAGBs). In general, the orientation angle of the low-angle grain boundaries is less than 15°, while the orientation angle of the high-angle grain boundaries is greater than 15° [18]. As can be seen from TABLE 1, the austenite content of the three specimens does not differ significantly, but the low and high-angle grain boundaries differ. The LAGBs dominate in the as-deposited and solid solution states, and the LAGBs are mainly distributed on the GBA and WA grains, while the HAGBs are mainly distributed on the contact interface between the ferrite and austenite phases. After tempering, the organization becomes homogeneous and the large-angle grain boundaries increase significantly. In general, HAGB has good resistance to deformation but poor corrosion resistance [19].

TABLE 1

Phase and LAGBs ratio of different treated samples

Sample	Austenite (%)		Ferrite (%)	
	Ratio	LAGBs Ratio	Ratio	LAGBs Ratio
As-deposited	62.8	89.1	37.2	94.4
Solid solution	63.8	83.9	36.2	90.6
Solid solution + Tempering	64.5	55.9	35.5	30.5

The Kernel Average Misorientation (KAM) measures the number of local particle dislocations, usually derived from EBSD data, and can be used to illustrate the local dislocation density [20]. The KAM distribution of the deposited and heat-treated samples is shown in Fig. 5, where it can be seen that the dislocation density of WAAM 2209 DSS decreases significantly after heat treatment due to the low temperature of tempering, and the dislocation density is consistent with solid solution.

3.2. Mechanical properties

Fig. 6 shows the mechanical properties of the 2009 DSS samples fabricated with the three different processes of arc additives. As can be seen from Fig. 6, the yield strength and tensile

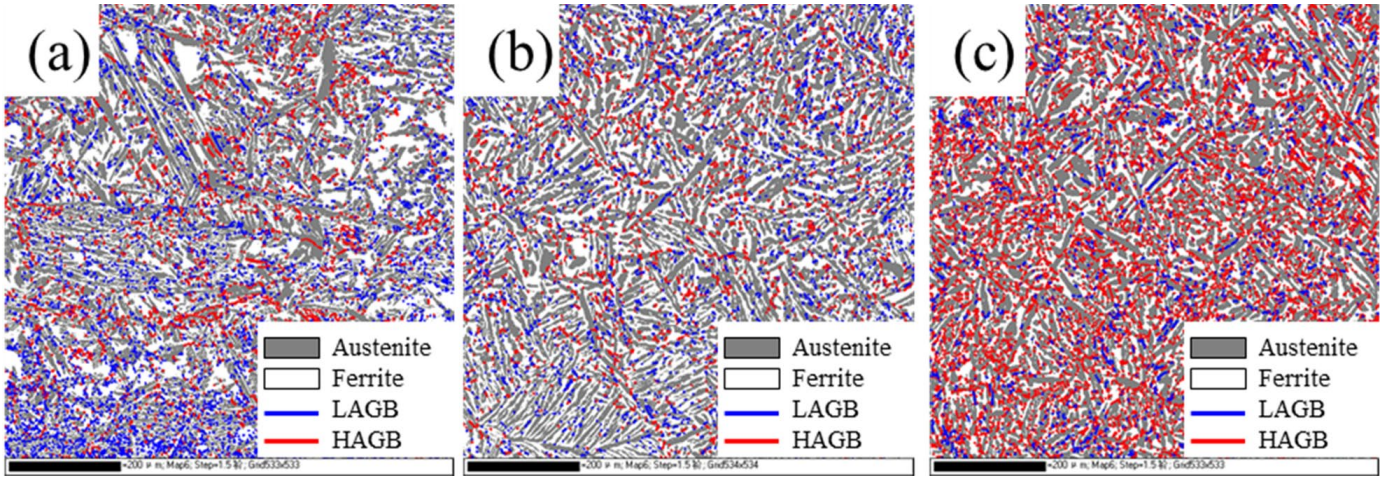

Fig. 4. Grain boundary characteristics of (a) as-deposited, (b) solid solution, (c) solid solution + tempering

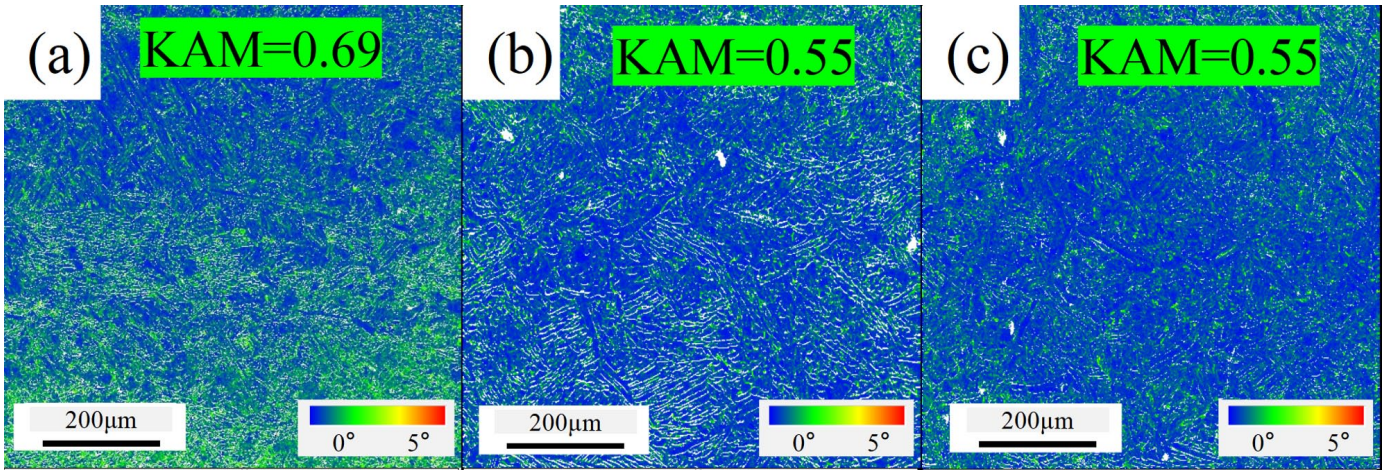

Fig. 5. KAM distribution of (a) as-deposited, (b) solid solution, (c) solid solution + tempering

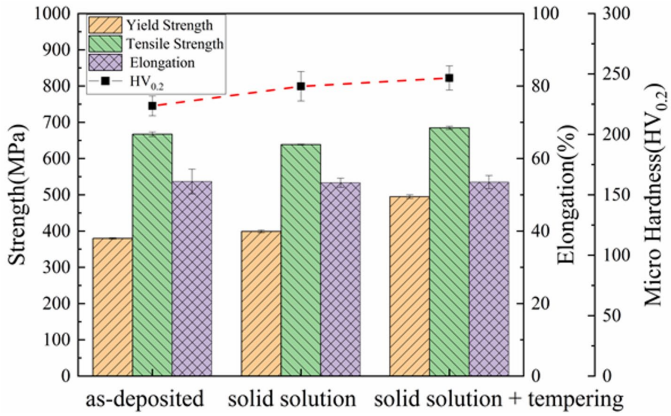

Fig. 6. Mechanical properties for the as-deposited, solid solution and solid solution + tempering

strength of the solid solution + tempered samples were the best, at 499.7 MPa and 687.7 MPa, respectively, with a 31.8% increase in yield strength and a slight increase in tensile strength compared to 379 MPa and 667 MPa in the deposited state. The mechanical properties of the solution heat treatment showed a slight decrease in tensile strength but an increase in yield strength compared to the original state. As shown in Fig. 6, the deposited, solid solution and solid solution + tempered samples all have good elongation, with elongation above 50%, which indicates that the 2209 DSS produced by arc additive manufacturing has good plasticity and does not reduce the elongation at break after heat treatment, while improving the strength of the material. Comparing the hardness in Fig. 6, it is found that the hardness of the samples after heat treatment has increased, and the average microhardness of the samples in the three treatment states are 223.6 HV, 240.2 HV and 245.6 HV, respectively, while the hardness of the solid solution + tempered state is 10% higher than the as-deposited state.

The fractures of the samples are shown in Fig. 7, and it can be clearly seen that all three samples exhibit toughness fracture with obvious dimples and tearing ridges. The size distribution of the dimples in the as-deposited samples is not uniform, but the presence of many fine γ_2 in itself contributes to the plastic toughness of the material. After heat treatment, the size of the dimples in the tissue became uniform, and the dimples combined with each other into an equiaxed dimple network, which enhanced the plastic toughness of the material.

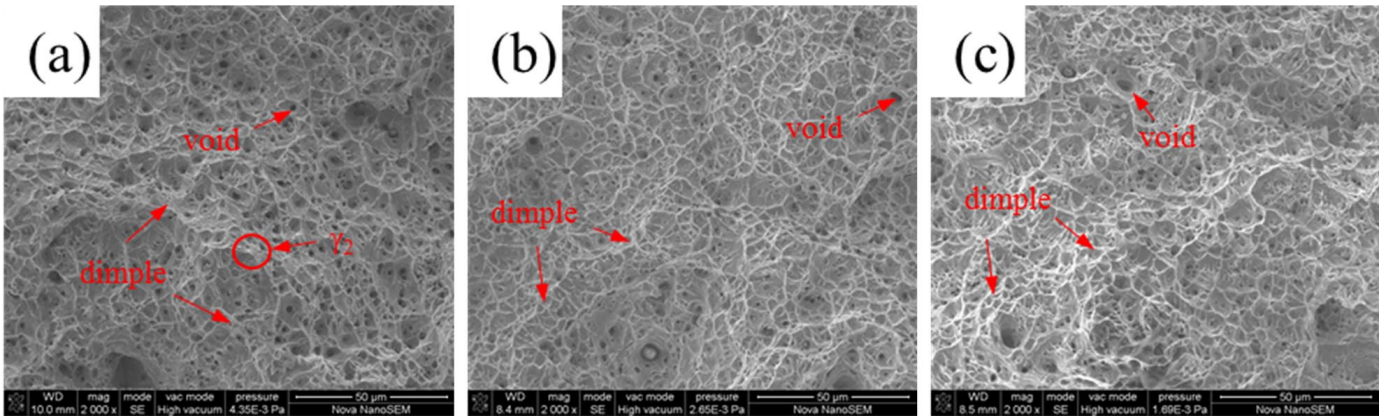

Fig. 7. The images of tensile fracture of samples under different condition: (a) as-deposited, (b) solid solution, (c) solid solution + tempering

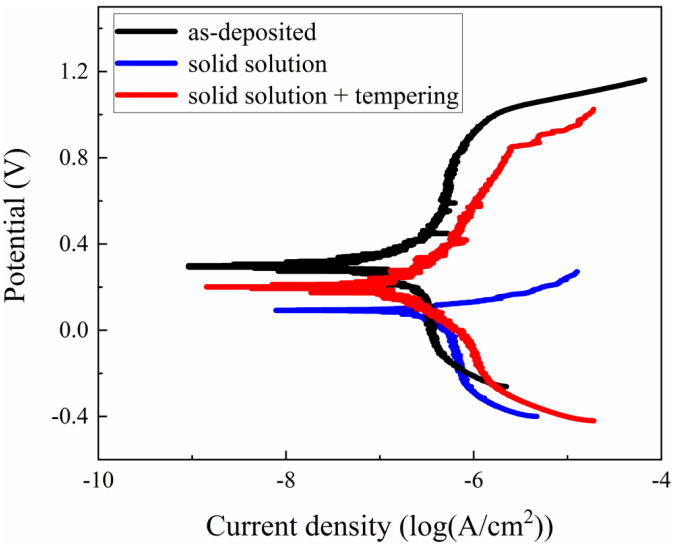

Fig. 8. Potentiodynamic polarization curves of the as-deposited and heat-treated WAAM DSS in 3.5 wt% NaCl solution

3.3. Electrochemical behavior

The polarization curves of the as-deposited and heat-treated WAAM DSS are shown in Fig. 8. In order to evaluate the corrosion characteristics of the specimens, the following electrochemical parameters were obtained: self-corrosion potential (*Ecorr*), self-corrosion current (*Icorr*) and passivation current density (*Ipass*), and the results are shown in TABLE 2. Theoretically, a higher *Ecorr* implies a lower electrochemical activity and a higher corrosion resistance [21]. However, the self-corrosion potential can only represent the corrosion resistance tendency of the material, while the self-corrosion current can indicate the actual corrosion rate of the material in solution. The magnitude of the passivation current density can reflect the stability of the material passivation film, and the higher the passivation current density indicates the poor stability of the passivation film. Among the as-deposited and heat-treated WAAM DSS samples, the highest *Ecorr* and the lowest *Icorr* and *Ipass* for the as-deposited

corrosion samples indicate that the as-deposited samples have good corrosion resistance and can quickly form a stable passivation film. After solid solution treatment, the corrosion resistance decreased, and there was no significant *Ipass*, but the corrosion resistance improved after further tempering treatment.

TABLE 2

Corrosion parameters of the polarization curves in 3.5 wt% NaCl solution

Sample	*Ecorr* / (V_{SCE})	*Icorr* / (A/cm^2)	*Ipass* / (A/cm^2)
As-deposited	0.299	5.42E-8	6.80E-7
solid solution	0.092	3.61E-7	—
solid solution + tempering	0.201	1.05E-7	2.58E-6

4. Discussion

The mechanism of σ-phase precipitation in DSS is related to γ_2, which is usually a co-precipitation reaction at the ferrite-austenite phase interface, where the precipitation of Cr-rich carbonation causes a decrease in the stability of ferrite and thus transforms into γ_2. The growth of γ_2 releases excess Cr, Mo and other elements in the phase, creating conditions for the precipitation of the σ-phase. A study by Westin [22] noted that the formation temperature of γ_2 is lower than that of primary austenite. Therefore, due to the non-isothermal thermal treatment, the samples in the original deposited state are prone to produce re-precipitated σ-phase at the grain boundaries. After solid solution treatment, the deleterious phase dissolves in the ferrite phase and the austenite distribution becomes homogeneous [23,24].

Due to the heat dissipation in the middle of WAAM with a specific orientation, the corresponding grains produced a particular selective orientation, as shown in Fig. 3. The solid solution treatment did not change the orientation of the austenite. However, after further tempering, it was found that the selective orientation disappeared and the grain orientation showed a random orientation. It is generally believed that low-temperature tempering does not change the grain orientation, which may be related to the selected location, such as the weld layer [25]. Solid solution treatment, on the one hand, eliminates thermal stresses, returns the distorted lattice, and recrystallizes the elongated and broken grains, but the tensile strength decreases and elongation increases; on the other hand, it maximizes the elimination of precipitation phases and improves the plasticity, toughness, and pitting resistance of DSS. Subsequent tempering improves tissue stability and eliminates internal stresses, while some fine-grained metal compounds will precipitate, which increases hardness and strength and hardens the specimen twice. The bright-field transmission images under different locations are shown in Fig. 9. In WAAM, firstly, many dislocations are accumulated inside the material under thermal stress. The density of dislocations gradually increases and entangles with each other to form dislocation walls, which can further develop into small-angle grain boundaries. Due to the low solid solution temperature, recrystallization is incomplete, which cannot effectively eliminate dislocations. Therefore, a large number of solute elements dissolved into the grain interior, causing lattice distortion, which is not conducive to corrosion performance. Small-angle grain boundaries are not stable, and after uniform tempering, they absorb dislocations and gradually transform into large-angle grain boundaries. Due to the austenite content being higher than 60%, these three specimens exhibit good plasticity. However, due to the inhomogeneous structure and thermal stress of the as-deposited sample, the deformation is uncoordinated, and the tendency of stress concentration is high during the tensile process, which results in a low yield strength.

5. Conclusions

In this paper, the effect of heat treatment on the tissue properties of 2209 DSS produced by arc additive manufacturing is investigated, and the conclusions can be drawn as follow:

(1) Heat treatment can effectively improve the grain inhomogeneity of WAAM 2209 DSS, reduce the amount of Weiss

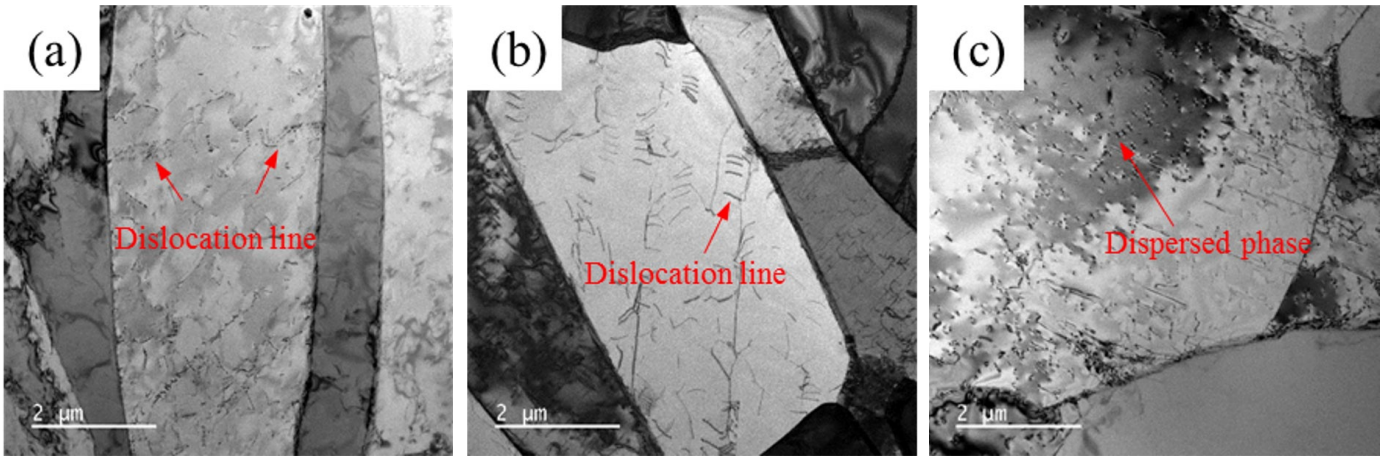

Fig. 9. Bright-field transmission images under different processing: (a) as-deposited, (b) solid solution, (c) solid solution + tempering

austenite, eliminate γ_2 and harmful brittle phases, and improve the mechanical properties of 2209 DSS.

(2) Solution heat treatment at 1100°C does not change the preferential grain orientation of austenite in the Z-direction, showing <101>//Z orientation distribution, but the preferential orientation disappears after solution + tempering heat treatment, which is related to the growth of grains. The deposited and solid solution states are mainly LAGBs. However, after tempering, the LAGBs absorb dislocations and become HAGBs, the number of HAGBs gradually increases, and the dislocation density decreases.

(3) The mechanical properties of the solid solution + tempered specimens were improved after heat treatment. The hardness, yield strength and tensile strength reached 245.6 HV, 499.7 MPa and 687.7 MPa, respectively, while having a good elongation of 52.5%. The hardness and yield strength increased by 10% and 31.8%, respectively, compared with the as-deposited state.

(4) The as-deposited sample has good corrosion performance, but the corrosion performance decreases after solid solution, and there is no apparent passivation zone. After solid solution + tempering, the corrosion performance was improved.

Acknowledgments

This work was jointly supported by grants from Anhui Provincial Natural Science Foundation (Grant No. 2108085ME173), Key Laboratory of Construction Hydraulic Robots of Anhui Higher Education Institutes, Tongling University (Grant No. TLXYCHR-O-21YB03), and open founds from Anhui Province Key Laboratory of Metallurgical Engineering & Resources Recycling (Grant No. SKF20-05).

REFERENCES

[1] S. Sasaki, T. Katsumura, J. Yanagimoto, Grain refinement technology for duplex stainless steel using rapid cooling immediately before hot working. J. Mater. Process. Tech. **281**, 116614 (2020). DOI: https://doi.org/10.1016/j.jmatprotec.2020.116614

[2] Y.Q. Wang, J. Han, H.C. Wu, B. Yang, X.T. Wang , Effect of sigma phase precipitation on the mechanical and wear properties of Z3CN20.09M cast duplex stainless steel. Nucl. Eng. Des. **259**, 1-7 (2013). DOI: http://dx.doi.org/10.1016/j.nucengdes.2013.02.037

[3] D. Zhang, A. Liu, B. Yin, P. Wen, Additive manufacturing of duplex stainless steels – A critical review. J. Manuf. Process. **73**, 496-517 (2022). DOI: https://doi.org/10.1016/j.jmapro.2021.11.036

[4] S.I. Evans, J. Wang, J. Qin, Y. He, P. Shepherd, J. Ding, A review of WAAM for steel construction – Manufacturing, material and geometric properties, design, and future directions. Structures **44**, 1506-1522 (2022). DOI: https://doi.org/10.1016/j.istruc.2022.08.084

[5] S. Singh, S.K. Sharma, D.W. Rathod, A review on process planning strategies and challenges of WAAM. Mater. Today Proc. **47**, 6564-6575 (2021). DOI: https://doi.org/10.1016/j.matpr.2021.02.632

[6] A. Rajesh Kannan, N. Siva Shanmugam, V. Rajkumar, M. Vishnukumar, Insight into the microstructural features and corrosion properties of wire arc additive manufactured super duplex stainless steel (ER2594). Mater. Lett. **270**, 127680 (2020). DOI: https://doi.org/10.1016/j.matlet.2020.127680

[7] B. Parvaresh, R. Miresmaeili, M. Yazdizadeh, Characterization of wire arc additive manufactured products: A comparison between as-deposited and inter-layer cold worked specimens, J. Manuf. Process. **57**, 61-71 (2020). DOI: https://doi.org/10.1016/j.jmapro.2020.05.053

[8] G. Posch, K. Chladil, H. ChladilL, Material properties of CMT – metal additive manufactured duplex stainless steel blade-like geometries, Weld World **61**, 873-882 (2017). DOI: https://doi.org/10.1007/s40194-017-0474-

[9] K. Wu, X. Hua, C. Shen, Y.N Ding, J. Xin, G. Mou, L. Wang, Y. Zhang, W. Zhou, K.M. Reddy, Effect of variable polarity during cold metal transfer on microstructure and mechanical properties of directed energy deposition-arc built 2209 duplex stainless steel. Addit. Manuf. 103750 (2023). DOI: https:// doi.org/10.1016/j.addma.2023.103750

[10] Y. Zhang, S. Wu, F. Cheng, A duplex stainless steel (DSS) with striking tensile strength and corrosion resistance produced through wire arc-additive manufacturing (WAAM) using a newly developed flux-cored wire. Mater. Lett. **313**, 131760 (2022). DOI: https://doi.org/10.1016/j.matlet.2022.131760

[11] P.P. Nikam, D. Arun, K.D. Ramkumar, N. Sivashanmugam, Microstructure characterization and tensile properties of CMT-based wire plus arc additive manufactured ER2594. Mater. Charact. **169**, 110671 (2020). DOI: https://doi.org/10.1016/j.matchar.2020.110671

[12] Z. Zhang, H. Jimg, L. Xu, Y. Han, L. Zhao, Effect of post-weld heat treatment on microstructure evolution and pitting corrosion resistance of electron beam-welded duplex stainless steel. Corros. Sci. **141**, 30-45 (2018). DOI: https://doi.org/10.1016/j.corsci.2018.06.030

[13] Z. Zhang, H. Zhao, H. Zhang, J. Hu, J. Jin, Microstructure evolution and pitting corrosion behavior of UNS S32750 super duplex stainless steel welds after short-time heat treatment. Corros Sci, **121**, 22-31 (2017). DOI: http://dx.doi.org/10.1016/j.corsci.2017.02.006

[14] S.T. Kim, S.H. Jang, I.S. Lee, Y.S. Park, Effects of solution heat-treatment and nitrogen in shielding gas on the resistance to pitting corrosion of hyper duplex stainless steel welds. Corros. Sci. **53**, 1939-4197 (2011). DOI: http://doi:10.1016/j.corsci.2011.02.013

[15] Y. Zhang, F. Cheng, S. Wu, Improvement of pitting corrosion resistance of wire arc additive manufactured duplex stainless steel through post-manufacturing heat-treatment. Mater. Charact. **171**, 110743 (2021). DOI: https://doi.org/10.1016/j.matchar.2020.110743

[16] A. Eghlimi, M. Shamanian, M. Eskandarian, A. Zabolian, J.A. Szpunar, Characterization of microstructure and texture across

dissimilar super duplex/austenitic stainless steel weldment joint by super duplex filler metal. Mate. Charact. **106**, 27-35 (2015). DOI: http://dx.doi.org/10.1016/j.matchar.2015.05.017

[17] Z. Zhang, H. Jing, L. Xu, Y. Han, L. Zhao, Influence of microstructure and elemental partitioning on pitting corrosion resistance of duplex stainless steel welding joints. Appl. Surf. Sci. **394**, 297-314 (2017).
DOI: http://dx.doi.org/10.1016/j.apsusc.2016.10.047

[18] Y. Zhang, S. Cheng, S. Wu, F. Chen, The evolution of microstructure and intergranular corrosion resistance of duplex stainless steel joint in multi-pass welding. J. Mater. Process. Technol. **277**, 116471 (2020).
DOI: https://doi.org/10.1016/j.jmatprotec.2019.116471

[19] Y. Shi, W. Li, L. Tian, Y. Sun, J. Zhang, H. Jing, L. Zhao, L. Xu, Y. Han, Effect of ferrite and grain boundary characteristics on corrosion properties of thermal simulated 316 L heat affected zone, Corros. Sci. **222**, 111384 (2023).
DOI: https://doi.org/10.1016/j.corsci.2023.111384

[20] M. Vishnukumar, V. Muthupandi, S. Jerome, Effect of post-heat treatment on the mechanical and corrosion behaviour of SS316L fabricated by wire arc additive manufacturing. Mater. Lett. **307**, 131015 (2022).
DOI: https://doi.org/10.1016/j.matlet.2021.131015

[21] L.N. Zhang, O.A. Ojo, Corrosion behavior of wire arc additive manufactured Inconel 718 superalloy. J. Alloys. Compd. **829**, 154455 (2020).
DOI: https://doi.org/10.1016/j.jallcom.2020.154455

[22] E. Westin, Microstructure and properties of welds in the lean duplex stainless steel LDX 2101. Metallurgi Och Metalliska Material, (2010).

[23] A.J. Ramirez, S.D. Brandi, J.C. Lippold, Secondary austenite and chromium nitride precipitation in simulated heat affected zones of duplex stainless steels. Sci. Technol. Weld. Joi. **9** (4), 301-13 (2013). DOI: https://doi: 10.1179/136217104225021715

[24] C.H.X.M. Magalhães, G.L.D. Faria, L.E. Lageiro, J.D. Silva, Characterization of the Austenite Reformation Mechanisms as a Function of the Initial Ferritic State in a UNS S32304 Duplex Stainless Steel. Mater. Res. **20** (6), 1470-1479 (2017).
DOI: http://dx.doi.org/10.1590/1980-5373-MR-2016-1122

[25] X. Zhang, K. Wang, Q. Zhou, J. Kong, Y. Peng, J. Ding, J. Diao, C. Diao, D. Yang, Y. Huang, T. Zhang, S.W. Williams, Element partitioning and electron backscatter diffraction analysis from feeding wire to as-deposited microstructure of wire and arc additive manufacturing with super duplex stainless steel. Mater. Sci. Eng. A **773**, 138856 (2020).
DOI: https://doi.org/10.1016/j.msea.2019.138856